



Optimization of laser beam parameters during processing of ASA 3D-printed plates

John D. Kechagias¹ · Konstantinos Ninikas¹ · Foteini Vakouftsi¹ · Nikolaos A. Fountas² · Sivasubramanian Palanisamy³ · Nikolaos M. Vaxevanidis²

Received: 7 September 2023 / Accepted: 22 November 2023 / Published online: 30 November 2023
© The Author(s) 2023

Abstract

New developments in manufacturing processes impose the need for experimental studies concerning the determination of beneficial process-related parameter settings and optimization of objectives related to quality and efficiency. This work aims to improve cutting geometry, surface texture, and arithmetic surface roughness average in the case of post-processing of filament material extrusion 3D-printed acrylonitrile styrene acrylate (ASA) thin plates by a low-power CO₂ laser cutting apparatus. This material was selected owing to its unique properties for thin-walled customized constructions. Three parameters, namely focal distance, plate thickness, and cutting speed, were examined with reference to the Box-Behnken design of experiments (BBD) and regression modeling. Four responses were considered: mean kerf width, W_m (mm); down width, W_d (mm); upper width, W_u (mm); and average surface roughness R_a (μm) of cut surfaces. Different regression models were tested for their efficiency in terms of predicting the objectives with an emphasis on full quadratic regression. The results showed that a focal distance of 6.5 mm and 16 mm/s speed optimizes all quality metrics for the three plate thicknesses. The regression models achieved adequate correlation among independent process-related parameters and optimization objectives, proving that they can be used to improve the laser cutting process and support practical applications.

Keywords CO₂ laser · Acrylonitrile styrene acrylate · Filament material extrusion · Box-Behnken design · Kerf geometry · Surface roughness · Regression

1 Introduction

Advances in material science and manufacturing technology have led to achievements related to part quality improvement with the simultaneous reduction of production time. Hybrid manufacturing [1, 2] is such an achievement that two or more subsequent manufacturing processes are integrated to produce competitive, complex components with great shape accuracy, quality of surface texture, and enhanced mechanical strength [3–5]. Laser processing applications in

3D-printed objects aim to refine either dimensional accuracy or surface texture, especially for thin-walled parts fabricated using fused deposition modeling (FDM) technology [6–8]. FDM technology or filament material extrusion (ME) currently introduces noticeable contributions to production branches [9–14] while it fosters novel applications engaging other manufacturing techniques, including laser processing. Nevertheless, significant drawbacks of ME technology span a number of defects related to shape deformations on parts' edges, shrinkage, deteriorated finishing details, and poor surface texture in different positioning aspects upon fabrication, i.e., flat inclined and vertical [15]. Challenging factors for successful operations regarding additive manufacturing (AM) include defining proper filament materials according to the application and specification of process-related thermo-mechanical parameters such as printing temperature and speed. Most applications related to fabricated parts using ME are post-processing, where finishing requirements should be achieved either by chemical treatments or machining [16–20]. Such post-processing treatments are applied

✉ John D. Kechagias
jkechag@uth.gr

¹ FWSD Department, University of Thessaly, GR, 43100 Karditsa, Greece

² Department of Mechanical Engineering, School of Pedagogical and Technological Education (ASPETE), 15122 Marousi, GR, Greece

³ Dilkap Research Institute of Engineering and Management Studies, Neral, Karjat, Maharashtra 410101, India

to most commercially available filament materials for fabricating different parts, adopting ME technology. Despite the numerous applications of well-known ME materials like acrylonitrile butadiene styrene (ABS) and polylactic acid (PLA) [21, 22], other materials exhibit research interest, such as acrylonitrile styrene (ASA) owing to its enhanced mechanical properties [23] including high glass transition temperature, ultraviolet resistance, environmental stability, and oil-heat resistance for preventing discoloration [24, 25].

Over the past few years, laser material processing (LMP) has been applied for post-processing and finishing operations in additively manufactured objects. In particular, research interest is given to post-processing techniques of thin ME plates where requirements related to cutting, polishing, engraving, and texturing requirements need to be met [26–28]. When it comes to surface texture characterization of polymeric thin plates [29], several attributes involving the laser process-related control parameters, i.e., focal length, laser power, and laser speed, as well as plate thickness, porosity, and density, should be explored under the goal of achieving high performance and safe application [30–32]. Process-related laser parameter investigation in the case of 3D-printed plate cutting is a relatively new research area since 3D printing technology introduces a wide range of materials with improved properties. These materials require different settings referring to process parameters such as layer deposition. Alternatives of process parameter setting affect the surface texture and porosity of finished components, affecting laser processing efficiency. In [33], CO₂ laser processing of 4-mm thick PLA 3D-printed plates was applied, and kerf properties were examined under different settings for laser speed and power. It was shown that when laser speed varies in a range of 8–18 mm/s, effects on kerf characteristics are considerably higher compared to those obtained when altering laser power settings within the range between 82.5 and 97.5 W. The importance of focal distance on upper kerf width variations was examined in [34]. Stavropoulos et al. [35] studied the effect of laser-based process parameters on various performance metrics for aerospace applications. In [36], significant aspects concerning laser technology are highlighted referring to the principal lasers employed for materials processing. In [37], a 30-W CO₂ laser processing apparatus working in continuous wave mode was implemented to treat the surface of PLA 3D-printed experimental specimens. The mechanism of surface finishing was investigated, and the effect of laser processing parameters, including scanning speed, energy density, and hatch distance, was identified in terms of surface topography. The results indicated that laser finishing significantly improved surface roughness, yet interactions among the process-related parameters involve surface ablation. By reviewing noticeable research contributions in the broader literature, it is evident that a high research interest

is focused on the experimental analysis and optimization of laser processing parameters, emphasizing thermoplastic and metallic materials [38–49].

Most laser processing research efforts emphasize parameter adjustment regarding kerf characteristics and cut surface texture for different materials and textures, underpinning the importance of laser cutting multi-objective optimization for customized or small-batch production of functional parts. Even if laser processing of metals, plastics, composites, etc., has been deeply investigated in the literature, 3D-printed plates made of ASA filament have not yet been studied. The last 3 years (2021–2023) of laser processing of thin polymeric materials have been reviewed, and the achievements in quality metrics are summarized in Table 1.

This work deals with a multi-objective optimization problem with reference to three independent process-related parameters referring to CO₂ laser cutting (focal distance, plate thickness, and laser speed) and two optimization objectives: kerf width and surface roughness in the case of the 3D-printed ASA thermoplastic filament as the work material to fabricate thin plates. Experimental runs were determined by adopting the Box-Behnken design of experiments (BBD) and response surface methodology (RSM). This work innovates and presents new experimental data for thin ASA samples that are 3D printed by applying ME technology while providing reliable results owing to the widespread Box-Behnken experimental design methodology.

2 Materials and methods

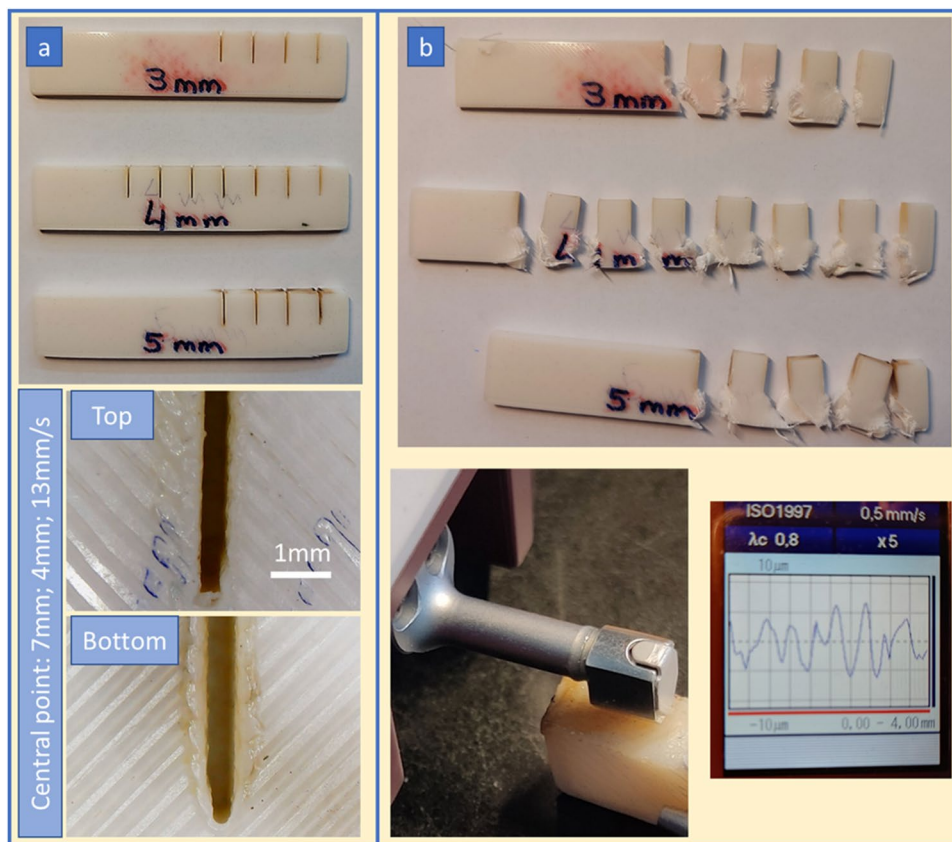
The ASA filaments used to 3D print the 3, 4, and 5-mm thick cuboidal samples (100-mm long and 20-mm wide; see Fig. 1a) were purchased from the market (NEEMA3D-ASA®; printing temperature range 135–255 °C, 1.75 mm in diameter, 1.1 g/cm³). The three specimens were 3D printed with ±45° raster orientation, 230 °C nozzle temperature, 30-mm/s printing speed, 0.3-mm layer thickness, 0.4-mm nozzle diameter, and 85 °C bed temperature.

The ASA 3D-printed plates were cut with the BCL 1325 Bodor continuous CO₂ laser (up to 150-W laser power). The BCL laser is equipped with a 2-mm tip conical convergent nozzle, three reflectors, and one focus lens for laser beam delivery, and it runs at a wavelength of 10.6 μm. The G-code programs were created with the RDWorks® 8.0 software. To modify the focal distance (or standoff distance) between the nozzle tip and the upper surface of the specimen, laser calibration spacers of 6-, 7-, and 8-mm height were utilized. The diameter of the beam spot on the upper surface of an 8-mm focal distance had the smallest value of 0.3 mm. It is also worth noting that even if the air pressure remains constant during the experiment (1 bar), any fluctuation in the focal length influences the distribution of air in the cutting area.

Table 1 Kerf geometry characteristics during laser cutting of polymeric plates

Material	Constant parameters	Variable parameters	Achievements/conclusions
PLA filament, 2021 [33]	CO ₂ laser 10.6 μm; stand of distance (SoD), 8 mm; gas pressure (GP), air 1 bar; plate thickness (PT), 4 mm; cuboid parts, 15 mm × 15 mm	Laser power (LP), 82.5–97.5 W; laser speed (LS), 8–18 mm/s	Kerf angle, between 0.884 and 1.653°; Ra, between 0.92 and 6.19 μm
PMMA plates, 2021 [6, 31]	CO ₂ laser 10.6 μm; GP, air 1 bar; PT, 4 mm; cuboid parts, 15 mm × 15 mm	SoD, 7–9 mm; LP, 82.5–97.5 W; LS, 8–18 mm/s; surface orientation; surface position on platform	Upper kerf width (Wu), 326–575 μm; down kerf width (Wd), 163–479 μm; Ra, 0.61–5.13 μm
PET-G filament, 2001 [50]	CO ₂ laser 10.6 μm; GP, air 1 bar; PT, 4 mm; cutting lines, 10 mm	SoD, 7–8 mm; LP, 82.5–97.5 W; LS, 8–18 mm/s	Wu, 272–510 μm; Wd, 251–498 μm; Ra, 7.17–11.988 μm
ABS filament, 2022 [51]	CO ₂ laser 10.6 μm; GP, air 1 bar; PT, 4 mm; cutting lines, 10 mm	SoD, 7–8 mm; raster angle (RA), 0–45–90°; LP, 82.5–97.5 W; LS: 8–18 mm/s	Wu, 321–722 μm; Wd, 181–965 μm; Ra, 3.018–7.804 μm
PLA/wood filament, 2022 [30, 52]	CO ₂ laser 10.6 μm; GP, air 1 bar; PT, 4 mm; cutting lines, 10 mm; SoD, 7 mm; wood content, 30 %	RA, 0–45–90°; LP, 82.5–97.5 W; LS, 8–18 mm/s	Mean kerf width (Wm), 331–690 μm; Ra, 6.012–11.451 μm
PLA/CNT filament, 2023 [34]	CO ₂ laser 10.6 μm; GP, air 1 bar; PT, 4 mm; cutting lines, 10 mm	CNT content, 0–2.5–5%; RA, 0–45–90°; LP, 82.5–105 W; LS, 3–18 mm/s; SoD, 6–9 mm	Wu, 410–1130 μm; Wd, 190–1120 μm; Ra, 3.70–11.60 μm
PLA/CB filament, 2023 [53]	CO ₂ laser 10.6 μm; GP, air 1 bar; PT, 4 mm; cutting lines, 10 mm	CB content, 0–2.5–5%; RA, 0–45–90°; LP, 82.5–105 W; LS, 3–18 mm/s; SoD, 6–9 mm	Wu, 420–1170 μm; Wd, 0.001–1190 μm; Ra, higher than 15 μm for 5% CB content
PE, PMMA, PP, PVC, pure plates, 2023 [54]	CO ₂ laser 10.6 μm; plate thickness, 4 mm; SoD, 8 mm; gas pressure, air 2 bar	LP, 80–140 W; CS, 1–6 mm/s	Optimization of roughness using neural networks and genetic algorithms. Average kerf deviations between 36 and 205 μm
PMMA pure, 2023 [55]	CO ₂ laser; channel profile study	LP, 30–60 W; LS, 25–200 mm/s	Developed models to estimate channel profile
PLA filament, 2023 [56]	Laser polishing of upper 3D-printed surfaces	LP, 3–30 W; LS, 50–500 mm/s	Surface roughness decrease of over 80% was achieved
PETG filament, 2023 [1]	Post-processing of the 3D printing hybridized method	(3D printing) Infill rate, 4–100 %; layer thickness, 0.1–0.3 mm; printing speed, 40–82 mm/s (Laser polishing) LS, 65–407 mm/s; LP, 10–20% (30 W)	58.38% reduction in surface roughness and an 8.8% increase in tensile strength is achieved

Fig. 1 a Specimens used for CO₂ laser cutting and upper and bottom kerf width characteristics and measurements (100-mm length; 20-mm width; and 3, 4, and 5 mm in thickness) and **b** roughness measurements on the cut surfaces



The cuts were 10-mm straight lines in the laser platform's Y-axis direction. After laser cutting, the upper (W_u , mm) and down (W_d , mm) kerf widths were measured at three distances. The average or mean kerf width was then calculated (W_m , mm). The upper and down kerf widths were measured using ImageJ® software. The average (mean) surface (R_a) was measured on the cut surfaces at 1 mm down the upper cutting edge by using a SurfTest SJ-210® profilometer, in the laser cut direction, see Fig. 1b.

The experimental design, known as the Box-Behnken design (BBD), and the response surface methodology (RSM) were accomplished to analyze and determine the association between the cutting performance and processing variables. The BBD is well suited to fit a second-order quadratic mathematical model (surface response), usually designed for process optimization. The three independent parameters were focal distance (A), plate thickness (B), and cutting speed (C). The kerf mean width (W_m , mm), down width (W_d , mm), upper width (W_u , mm), and average surface roughness of the cut surfaces (R_a , μm) observed from each experiment were used as the response value. The variable levels were coded as -1 , 0 , and $+1$. These three codes were spread out equally. The variables and their affiliated coded and actual

levels decided in the three-factor-three-level BBD design are shown in Table 2. The variables' ranges were selected from preliminary experiments, which found that focal distance, plate thickness, and cutting speed significantly affect the laser cutting efficiency. The laser power was kept constant at the higher 100% values close to 150 W.

3 Results and discussion

The Box-Behnken design of experiments (BBD) is suggested in the literature as an appropriate design for fitting a full quadratic model to the observed results [57–59]. Generally, in stochastic problems such as laser cutting of thin

Table 2 Process parameters, levels, and codes

Variables	Codes	Levels and range		
		-1	0	1
Focal distance (mm)	<i>A</i>	6	7	8
Plate thickness (mm)	<i>B</i>	3	4	5
Cutting speed (mm/s)	<i>C</i>	8	13	18

plates, the processing parameters are first sorted, and the center point and the number of experiment repetitions at the center point are defined, followed by the selection of the upper and lower levels of the variable parameters [60, 61]. Second, the experimental array and run order should be determined, considering that all experiments should be run. Second-order models should then be tested for goodness-of-fit according to the Darling-Anderson validity test (residual normality test) [62–64]. Finally, the results are decoded using the contour plots and response surfaces between parameter pairs according to each performance metric [65–67].

Due to its robustness, the BBD methodology is used for various optimization case studies of technology problems. The most widely applied experimental BBD array uses three variables and 15 experiments with three replications at the central point [68]. Following the above methodology, lower values (−1 code) of 6 mm A (focal distance), 3 mm B (plate thickness), and 8 mm/s C (cutting speed) were selected; maximum values (1 code) of 8 mm A, 5 mm B, and 18 mm/s C; and central values (0 code) of 4 mm A, 4 mm B, and 13 mm/s C (see Table 2). Therefore, Table 3 is constructed and implemented in the laser cutting experiments.

Fitting the input variables (X_i ; here A, B, and C) with the output variables (Y_k ; here Wm, Wd, Wu, and Ra) with a quadratic regression model means that a multi-parameter equation with linear (b_i), cross (b_{ij}), and quadratic (b_{ii}) products are assigned between X_i inputs and Y_k outputs (Eq. 1; [69]):

$$Y_k = b_0 + \sum_i b_i X_i + \sum_{i \neq j} b_{ij} X_i X_j + \sum_i b_{ii} X_i^2 \pm e \tag{1}$$

In experimental studies that are characterized as stochastic problems, it is suggested in the literature to test the model’s goodness of fit by applying the Anderson-Darling normality test to the residuals. Figure 2a–d shows that the residuals Wm, Wd, Wu, and Ra follow the normal distribution, having p -values higher than 0.05, thus proving the validity of the Box-Behnken methodology.

ANOVA (variances analysis) is a statistical analysis that examines the experimentally observed and predicted quadratic model value differences. Here, the Rsq values of the Wm, Wd, Wu, and Ra models are 88.06%, 90.19%, 86.94%, and 74.93%, with standard deviations (S) of 0.0338, 0.0392, 0.0334, and 1.020, respectively (see Tables 4, 5, 6 and 7).

The regression full second-order models for each metric follow:

$$\begin{aligned} Wm = & -1.23 + 0.513 \times A - 0.119 \times B \\ & + 0.0082 \times C - 0.0383 \times A^2 + 0.0100 \times B^2 \\ & + 0.000912 \times C^2 + 0.0203 \times AB - 0.00200 \\ & \times AC - 0.00678 \times BC \end{aligned} \tag{2}$$

$$\begin{aligned} Wd = & -3.42 + 1.112 \times A - 0.088 \times B \\ & + 0.0180 \times C - 0.0816 \times A^2 \\ & + 0.0084 \times B^2 + 0.001298 \\ & \times C^2 + 0.0236 \times AB - 0.00367 \\ & \times AC - 0.00907 \times BC \end{aligned} \tag{3}$$

Table 3 Box-Behnken design: control parameters, levels and outputs (Wm, Wd, Wu, and Ra)

Run order	Input variables (X_i)			Output variables (Y_k)			
	A, focal distance (mm)	B, plate thickness (mm)	C, cutting speed (mm/s)	Wm (mm)	Wd (mm)	Wu (mm)	Ra (μ m)
1	6	4	8	0.412	0.388	0.436	5.072
2	7	5	8	0.597	0.622	0.573	2.918
3	8	5	13	0.489	0.445	0.533	2.670
4	7	4	13	0.454	0.431	0.476	3.824
5	8	4	8	0.528	0.489	0.567	2.106
6	6	3	13	0.412	0.366	0.458	2.173
7	8	4	18	0.454	0.387	0.521	3.525
8	7	3	8	0.516	0.509	0.524	3.366
9	6	5	13	0.417	0.400	0.433	4.962
10	7	4	13	0.456	0.462	0.450	4.981
11	7	3	18	0.453	0.460	0.446	1.956
12	7	4	13	0.466	0.472	0.460	3.841
13	6	4	18	0.378	0.360	0.396	4.558
14	8	3	13	0.403	0.316	0.490	5.704
15	7	5	18	0.398	0.392	0.405	2.595

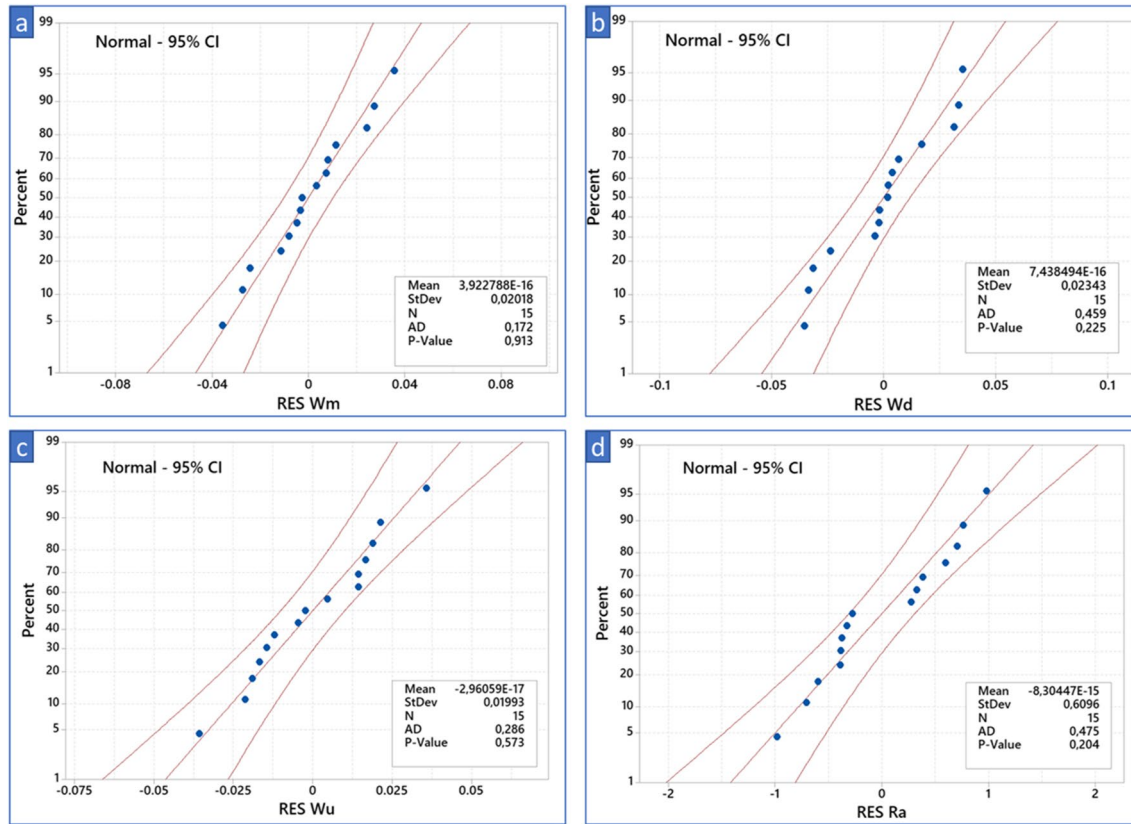


Fig. 2 Residual normality test for **a–c** residuals of mean (Wm), down (Wd), and upper (Wu) kerf widths, respectively, and **d** residuals of average surface roughness (Ra)

Table 4 2nd order model analysis: Wm versus A, B, and C

Source	DF	Adj SS	Adj MS	F-value	p-value
Model	9	0.042016	0.004668	4.10	0.067
A	1	0.004472	0.004472	3.92	0.104
B	1	0.000454	0.000454	0.40	0.556
C	1	0.000070	0.000070	0.06	0.814
A ²	1	0.005420	0.005420	4.76	0.081
B ²	1	0.000371	0.000371	0.33	0.593
C ²	1	0.001922	0.001922	1.69	0.251
AB	1	0.001647	0.001647	1.45	0.283
AC	1	0.000400	0.000400	0.35	0.579
BC	1	0.004601	0.004601	4.04	0.101
Error	5	0.005699	0.001140		
Lack-of-fit	3	0.005616	0.001872	45.29	0.022
Pure error	Error	2	0.000083	0.000041	
Total	14	0.047715			
R ²					88.06%
S					0.0338

Table 5 2nd order model analysis: Wd versus A, B, and C

Source	DF	Adj SS	Adj MS	F-value	p-value
Model	9	0.070636	0.007848	5.11	0.044
A	1	0.020977	0.020977	13.65	0.014
B	1	0.000248	0.000248	0.16	0.705
C	1	0.000341	0.000341	0.22	0.657
A ²	1	0.024601	0.024601	16.01	0.010
B ²	1	0.000259	0.000259	0.17	0.698
C ²	1	0.003890	0.003890	2.53	0.172
AB	1	0.002225	0.002225	1.45	0.283
AC	1	0.001344	0.001344	0.87	0.393
BC	1	0.008220	0.008220	5.35	0.069
Error	5	0.007685	0.001537		
Lack-of-fit	3	0.006791	0.002264	5.07	0.169
Pure error	Error	2	0.000894	0.000447	
Total	14	0.078321			
R ²					90.19%
S					0.0392

Table 6 2nd order model analysis: Wu versus A, B, and C

Source	DF	Adj SS	Adj MS	F-value	p-value
Model	9	0.037034	0.004115	3.70	0.082
A	1	0.000123	0.000123	0.11	0.753
B	1	0.000723	0.000723	0.65	0.457
C	1	0.000003	0.000003	0.00	0.961
A ²	1	0.000092	0.000092	0.08	0.785
B ²	1	0.000503	0.000503	0.45	0.531
C ²	1	0.000640	0.000640	0.58	0.482
AB	1	0.001156	0.001156	1.04	0.355
AC	1	0.000011	0.000011	0.01	0.924
BC	1	0.002025	0.002025	1.82	0.235
Error	5	0.005562	0.001112		
Lack-of-fit	3	0.005207	0.001736	9.78	0.094
Pure error	Error	2	0.000355	0.000177	
Total	14	0.042596			
R ²					86.94%
S					0.0334

Table 7 2nd order model analysis: Ra versus A, B, and C

Source	DF	Adj SS	Adj MS	F-value	p-value
Model	9	15.5470	1.72745	1.66	0.299
A	1	0.0228	0.02284	0.02	0.888
B	1	7.4103	7.41025	7.12	0.044
C	1	0.0105	0.01048	0.01	0.924
A ²	1	0.5454	0.54540	0.52	0.502
B ²	1	1.9256	1.92563	1.85	0.232
C ²	1	2.2705	2.27046	2.18	0.200
AB	1	8.4768	8.47683	8.15	0.036
AC	1	0.9351	0.93509	0.90	0.387
BC	1	0.2959	0.29594	0.28	0.617
Error	5	5.2028	1.04057		
Lack-of-fit	3	4.3233	1.44111	3.28	0.243
Pure error	Error	2	0.8795	0.43976	
Total	14	20.7499			
R ²					74.93%
S					1.020

$$\begin{aligned}
 Wu = & 0.95 - 0.085 \times A - 0.151 \times B - 0.0017 \\
 & \times C + 0.0050 \times A^2 + 0.0117 \times B^2 + 0.000527 \\
 & \times C^2 + 0.0170 \times AB - 0.00033 \\
 & \times AC - 0.00450 \times BC
 \end{aligned}
 \tag{4}$$

$$\begin{aligned}
 Ra = & -20.2 - 1.16 \times A + 15.25 \times B - 0.100 \\
 & \times C + 0.384 \times A^2 - 0.722 \\
 & \times B^2 - 0.0314 \times C^2 - 1.456 \\
 & \times AB + 0.097 \times AC + 0.054 \times BC
 \end{aligned}
 \tag{5}$$

The *F*-value and the *p*-value are the metrics that indicate the accuracy of the adopted second-order mathematical models, and it is desirable to have *F* > 4 and *p* < 0.05. Here, the Wm, Wd, and Wu models' *F*-values (4.10, 5.11, and 3.70) and *p*-values (0.067, 0.044, and 0.082) are close to or higher than the values mentioned above, having predicting accuracy higher than 85%. At the same time, the Ra has an *F*-value of 1.727, a *p*-value of 0.299, and an accuracy higher than 74%. It is characteristic here that the normality test of all metrics (Fig. 2a–d) shows that the second-order models can be used to indicate the parameters' main effect plots that are presented in Fig. 3a–d for all metrics.

The following conclusions can be drawn by studying the main effects plots (Fig. 3a–d):

- The focal distance between 6 and 6.5 mm increases the mean, down, and upper kerf widths, while the surface roughness was optimized for focal lengths between 7 and 7.5 mm. Note that the surface roughness measured 1 mm deeper than the upper plate surface for all three plate thicknesses. The focal distance affects the beam spot diameter and redistributes the energy and pressure air inside the kerf geometry, considerably improving laser cut efficiency when optimized.
- The 3-mm plate thickness optimizes the mean and down kerf width, which has the lower penetration depth (3 mm) and follows the literature. In contrast, the upper kerf width is optimized between 3.5 and 4-mm plate thickness. On the other hand, the surface roughness is optimized for 3 or 5-mm plate thicknesses.
- When the cutting speed increases, the mean, down, and upper kerf widths decrease, which is explained by the reduction of energy inserted per time unit inside the kerf geometry, resulting in lower kerf widths. On the other hand, reducing the power per unit time redistributes the energy and air pressure inside the kerf geometry in such a way that the surface roughness is optimized at higher cutting speeds.

In Figs. 4 and 5, the contour and surface plots are presented in order to apprehend the effects of the parameters on the laser cutting kerf characteristics.

From the contour and 3D surface plots (see Figs. 4 and 5), the following conclusions can be drawn about parameter interactions:

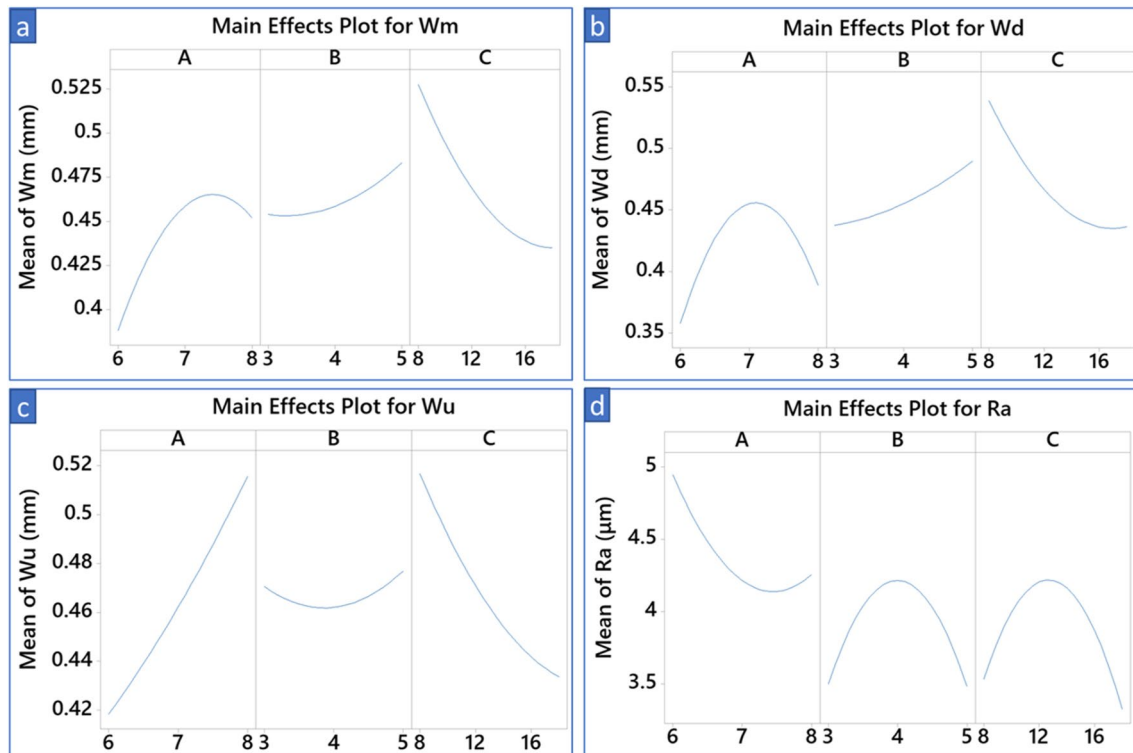


Fig. 3 Main effect plots based on second-order models for **a–c** mean (Wm), down (Wd), and upper (Wu) kerf widths, respectively, and **d** average surface roughness (Ra)

- The focal distance and plate thickness interactions ($B \times A$) at the center experimental point (7-mm focal distance, 4-mm plate thickness, and 13-mm/s cutting speed) indicate that values close to 6-mm focal distance and plate thickness close to 3 mm optimize all kerf widths (Wm, Wd, and Wu). In contrast, lower or higher focal lengths and plate thicknesses achieve the lowest Ra values.
- The focal distance and cutting speed interactions ($C \times A$) at the center experimental point (7-mm focal distance, 4-mm plate thickness, and 13-mm/s cutting speed) indicate that lower focal distance and higher cutting speed result in smaller kerf widths (Wm, Wd, and Wu) and Ra values.
- Finally, the cutting speed and plate thickness interactions ($C \times B$) at the center experimental point (7-mm focal distance, 4-mm plate thickness, and 13-mm/s cutting speed) indicate that higher values of cutting speed and plate thickness reduce the kerf widths (Wm, Wd, and Wu) and surface roughness (Ra) values.

Last but not least, by utilizing the second-order regression models and setting as criteria the optimization of mean width (Wm between 0.3 and 0.45) and surface roughness (Ra between 1 and 4 μm) with equal importance, the three below contour plots are extracted, which show the optimized area for the cutting speed and focal length values. Again, this plot confirms that the higher cutting speed and the lower focal distance results optimize the cutting process (mean kerf width lower than 0.45 mm and Ra values lower than 4 μm) (Fig. 6).

4 Conclusions

This work presented results concerning the experimental analysis of the effects of three crucial control parameters related to CO₂ laser cutting of 3D-printed ASA thin plates: focal length, plate thickness, and cutting speed. A series of experiments were established by adopting the Box-Behnken

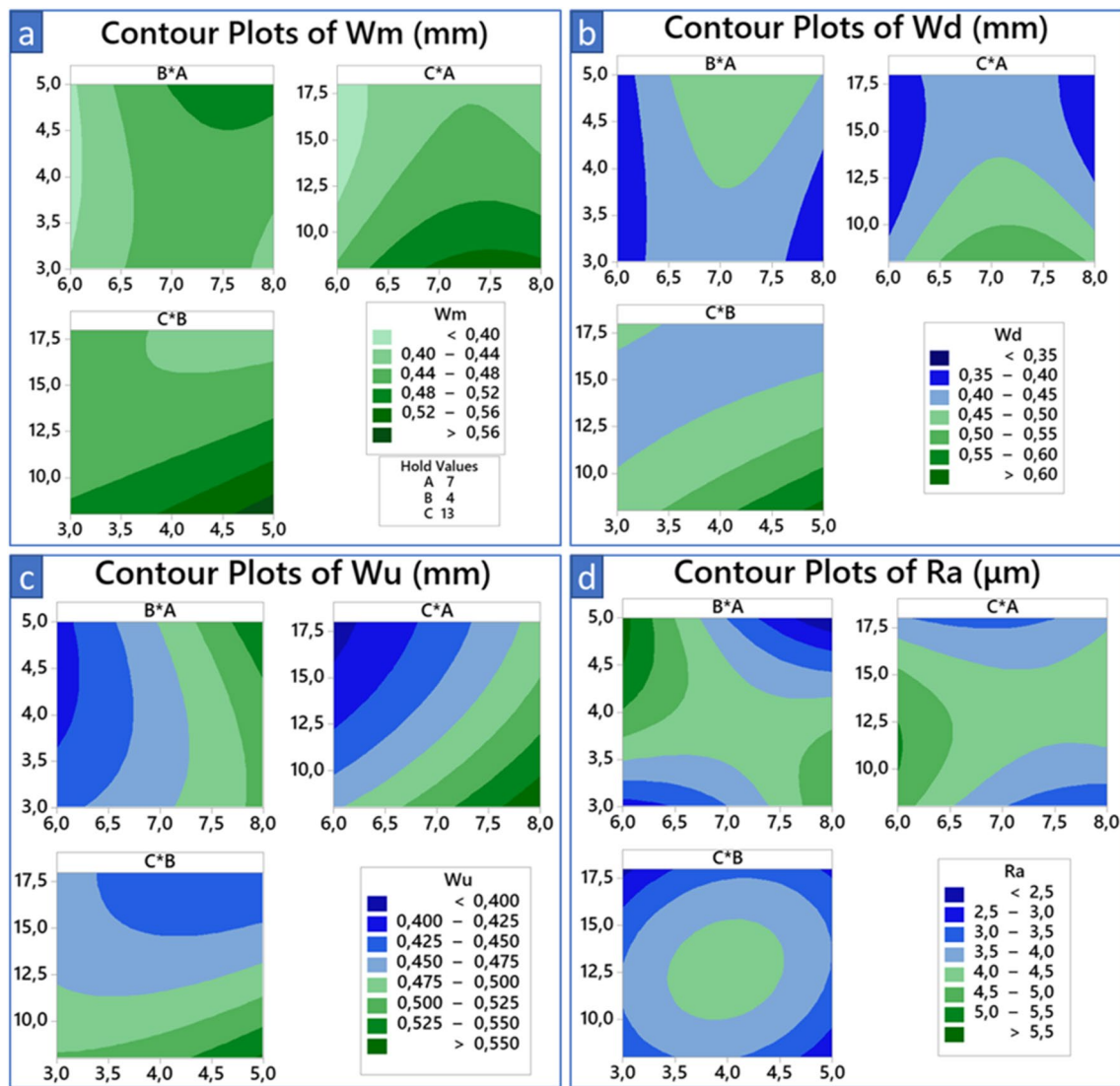


Fig. 4 Contour plots for **a–c** mean (Wm), down (Wd), and upper (Wu) kerf widths, respectively, and **d** average surface roughness (Ra)

design, thus coping with fewer experiments without losing essential information. Results showed that low settings for focal distance (i.e., close to 6.5 mm) seem advantageous in the laser cutting process, resulting in low surface roughness and mean kerf outputs (lower than 4 μm and 0.45 mm, respectively). Additional observations have shown that an operational range for cutting speed between 16 and 16.5 mm maintains mean kerf width and surface roughness in the same range (i.e., Wm lower than 0.45 mm and Ra lower than 4

μm). Reduced plate thickness (i.e., 0.3 mm) results in finer kerf widths and Ra values as expected, owing to lower penetration depth.

Box-Behnken experimental design and response surface methodology can be efficiently employed to analyze and optimize stochastic problems such as laser cutting of thin plates fabricated using cutting-edge 3D printing processes. From an overall point of view, this work demonstrated the complexity of these critical parameters, focal distance, plate

Fig. 5 Surface plots for **a–c** mean kerf (Wm), **d–f** down kerf width (Wd), **g–i** upper kerf width (Wu), and **k–m** average surface roughness (Ra)

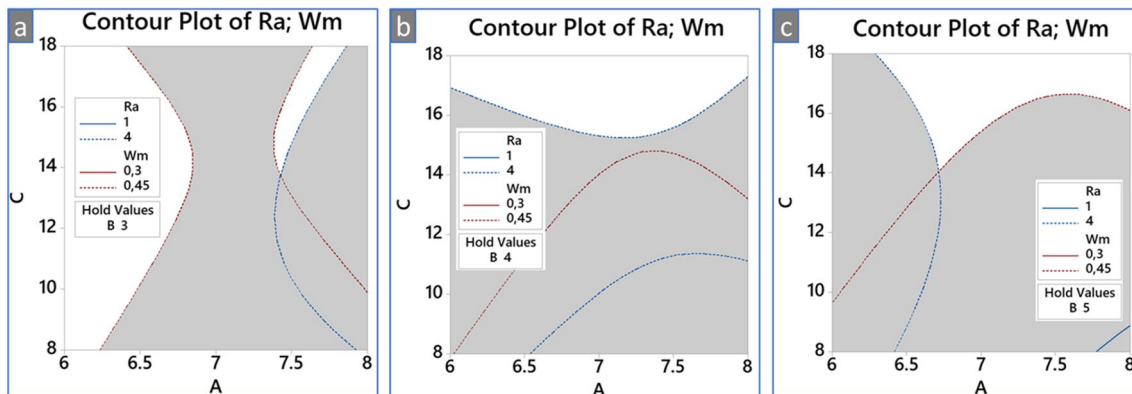
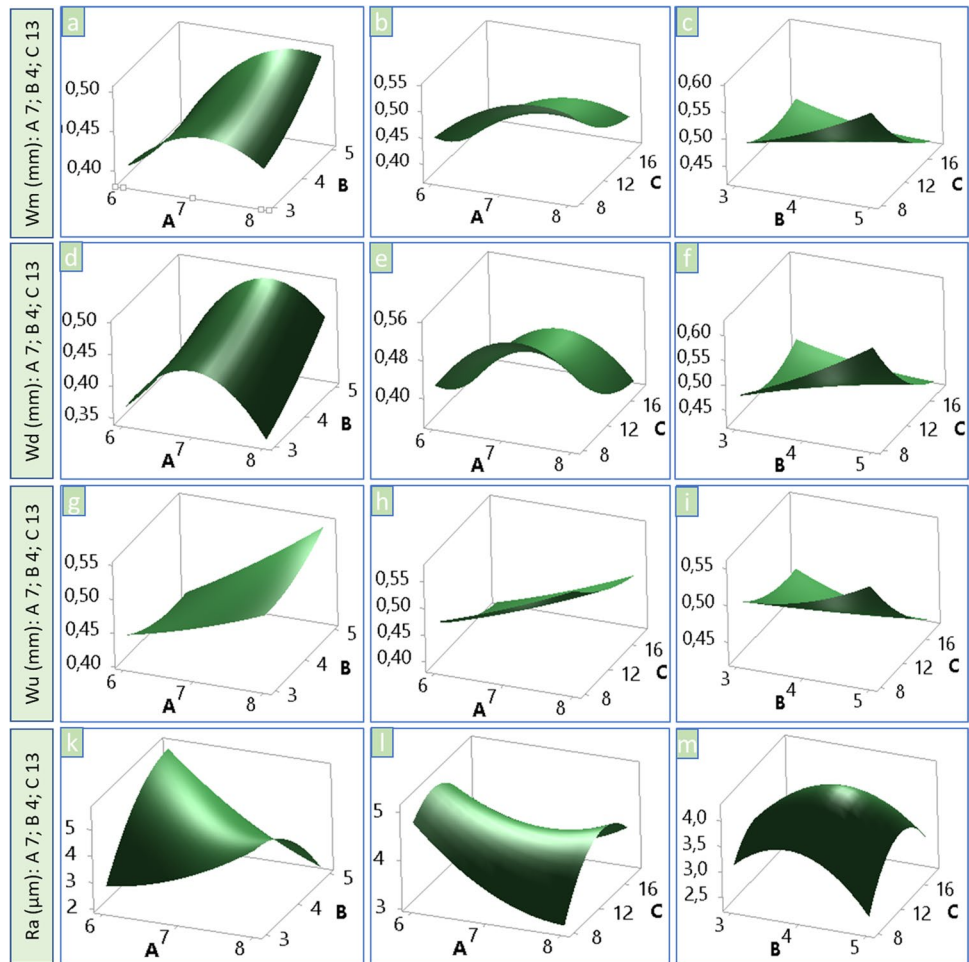


Fig. 6 Contour plots with $Ra < 4 \mu\text{m}$ versus $Wm < 0.45 \text{ mm}$ for **a** 3-mm plates, **b** 4-mm plates, and **c** 5-mm plates

thickness, and cutting speed, implying that multi-parameter, multi-objective optimization of laser cutting is an essential research task.

Nevertheless, a larger set of experimental results should be obtained to generate robust regression models further to establish a solid experimentation ground and reliably

study optimization potentials regarding CO_2 laser cutting of 3D-printed parts. Looking further ahead, the authors plan to conduct such an experimental set with different filaments and analyze the findings under the major scope of applying different optimization approaches like artificial neural networks and genetic algorithms for presenting

results that will facilitate industrial applications and support decision-making in practice.

Author contributions JK: methodology, conceptualization, writing (review and editing), resources, and supervision; KN: data curation; FV: data analysis; NF: software, writing (draft and editing); SP: visualization; NMV: writing (review and editing) and supervision.

Funding Open access funding provided by HEAL-Link Greece.

Data availability All data required to reproduce these findings are included in this manuscript

Declarations

Competing interests The authors declare no competing interests.

Open Access This article is licensed under a Creative Commons Attribution 4.0 International License, which permits use, sharing, adaptation, distribution and reproduction in any medium or format, as long as you give appropriate credit to the original author(s) and the source, provide a link to the Creative Commons licence, and indicate if changes were made. The images or other third party material in this article are included in the article's Creative Commons licence, unless indicated otherwise in a credit line to the material. If material is not included in the article's Creative Commons licence and your intended use is not permitted by statutory regulation or exceeds the permitted use, you will need to obtain permission directly from the copyright holder. To view a copy of this licence, visit <http://creativecommons.org/licenses/by/4.0/>.

References

- Mushtaq RT, Iqbal A, Wang Y, Khan AM, Abu Bakar MS (2023) Parametric optimization of 3D printing process hybridized with laser-polished PETG polymer. *Polym Test* 125:108129. <https://doi.org/10.1016/j.polymertesting.2023.108129>
- Dilberoglu UM, Gharehpapagh B, Yaman U, Dolen M (2021) Current trends and research opportunities in hybrid additive manufacturing. *Int J Adv Manuf Technol* 113:623–648. <https://doi.org/10.1007/s00170-021-06688-1>
- Cao D (2023) Fusion joining of thermoplastic composites with a carbon fabric heating element modified by multiwalled carbon nanotube sheets. *Int J Adv Manuf Technol* 128:4443–4453. <https://doi.org/10.1007/s00170-023-12202-6>
- Cao D, Bouzolin D, Lu H, Griffith DT (2023) Bending and shear improvements in 3D-printed core sandwich composites through modification of resin uptake in the skin/core interphase region. *Compos Part B Eng* 264:110912. <https://doi.org/10.1016/j.compositesb.2023.110912>
- Cao D (2023) Enhanced buckling strength of the thin-walled continuous carbon fiber-reinforced thermoplastic composite through dual coaxial nozzles material extrusion process. *Int J Adv Manuf Technol* 128:1305–1315. <https://doi.org/10.1007/s00170-023-12014-8>
- Kechagias J, Ninikas K, Stavropoulos P, Salonitis K (2021) A generalised approach on kerf geometry prediction during CO₂ laser cut of PMMA thin plates using neural networks, lasers manuf. *Mater Process* 8. <https://doi.org/10.1007/s40516-021-00152-4>
- Shirinbayan M, Benfriha K, Tcharkhtchi A (2022) Geometric accuracy and mechanical behavior of PA6 composite curved tubes fabricated by fused filament fabrication (FFF). *Adv Eng Mater* 24:2101056. <https://doi.org/10.1002/adem.202101056>
- Shakeri Z, Benfriha K, Zirak N, Shirinbayan M (2022) Mechanical strength and shape accuracy optimization of polyamide FFF parts using grey relational analysis. *Sci Rep* 12:13142. <https://doi.org/10.1038/s41598-022-17302-z>
- Akhoundi B, Ouzah R (2023) Experimental and numerical investigation of rotating bending fatigue of polylactic acid 3D printed parts by an extrusion-based additive manufacturing method. *J Eng Res*. <https://doi.org/10.1016/j.jer.2023.07.006>
- Akhoundi B, Sousani F (2023) An experimental investigation of screw-based material extrusion 3D printing of metallic parts. *J Eng Res*:100102. <https://doi.org/10.1016/j.jer.2023.100102>
- Thompson MS (2022) Current status and future roles of additives in 3D printing—a perspective. *J Vinyl Additive Technol* 28:3–16. <https://doi.org/10.1002/vnl.21887>
- Msallem B, Sharma N, Cao S, Halbeisen FS, Zeilhofer H-F, Thieringer FM (2020) Evaluation of the dimensional accuracy of 3D-printed anatomical mandibular models using FFF, SLA, SLS, MJ, and BJ printing technology. *J Clin Med* 9:817. <https://doi.org/10.3390/jcm9030817>
- Spahiu T, Canaj E, Shehi E (2020) 3D printing for clothing production. *J Eng Fiber Fabr* 15:155892502094821. <https://doi.org/10.1177/1558925020948216>
- Roach DJ, Roberts C, Wong J, Kuang X, Kovitz J, Zhang Q, Spence TG, Qi HJ (2020) Surface modification of fused filament fabrication (FFF) 3D printed substrates by inkjet printing polyimide for printed electronics. *Addit Manuf* 36:101544. <https://doi.org/10.1016/j.addma.2020.101544>
- Kechagias JD, Zaoutsos SP (2023) An investigation of the effects of ironing parameters on the surface and compression properties of material extrusion components utilizing a hybrid-modeling experimental approach. *Progr Additive Manuf*. <https://doi.org/10.1007/s40964-023-00536-2>
- Divis J, Hlosta J, Zurovec D, Rozbroj J, Kruszelnicka W, Necas J, Zegzulka J (2022) 3D printed laboratory equipment to measure bulk materials in extreme conditions. *Sci Rep* 12:17331. <https://doi.org/10.1038/s41598-022-22114-2>
- Kechagias J, Chaidas D (2023) Fused filament fabrication parameter adjustments for sustainable 3D printing. *Mater Manuf Process*:1–8. <https://doi.org/10.1080/10426914.2023.2176872>
- Bikas H, Stavropoulos P, Chryssolouris G (2016) Additive manufacturing methods and modelling approaches: a critical review. *Int J Adv Manuf Technol* 83:389–405. <https://doi.org/10.1007/s00170-015-7576-2>
- Dizon JRC, Gache CCL, Cascolan HMS, Cancino LT, Advincula RC (2021) Post-processing of 3D-printed polymers. *Technol (Basel)* 9:61. <https://doi.org/10.3390/technologies9030061>
- Kechagias JD, Fountas NA, Ninikas K, Vaxevanidis NM (2023) Kerf geometry and surface roughness optimization in CO₂ Laser Processing of FFF plates utilizing neural networks and genetic algorithms approaches. *J Manuf Mater Proc* 7:77. <https://doi.org/10.3390/jmmp7020077>
- El Magri A, Ouassil S, Vaudreuil S (2022) Effects of printing parameters on the tensile behavior of 3D -printed acrylonitrile styrene acrylate (ASA) material in Z direction. *Polym Eng Sci* 62:848–860. <https://doi.org/10.1002/pen.25891>
- Samykan M, Selvamani SK, Kadirgama K, Ngui WK, Kanagaraj G, Sudhakar K (2019) Mechanical property of FDM printed ABS: influence of printing parameters. *Int J Adv Manuf Technol* 102:2779–2796. <https://doi.org/10.1007/s00170-019-03313-0>
- Rakshit R, Kalvettakaran P, Acharyya SK, Panja SC, Misra D (2023) Development of high specific strength acrylonitrile styrene acrylate (ASA) structure using fused filament fabrication. *Progr Additive Manuf*. <https://doi.org/10.1007/s40964-023-00420-z>

24. Captan Prabakaran A, Senthil P, Sathies T (2023) Experimental and numerical investigations on the fatigue characteristics of FFF-printed acrylonitrile styrene acrylate parts. *Progr Additive Manuf*. <https://doi.org/10.1007/s40964-023-00432-9>
25. Siemiński P (2021) Introduction to fused deposition modeling. In: *Additive Manufacturing*. Elsevier, pp 217–275. <https://doi.org/10.1016/B978-0-12-818411-0-00008-2>
26. Kumbhar NN, Mulay AV (2018) Post processing methods used to improve surface finish of products which are manufactured by additive manufacturing technologies: a review. *J Instit Eng (India): Series C* 99:481–487. <https://doi.org/10.1007/s40032-016-0340-z>
27. Chai Y, Chen X-B, Zhang D, Lynch J, Birbilis N, Qin Q-H, Smith PN, Li RW (2020) Laser polished fused deposition poly-lactic acid objects for personalized orthopaedic application. *SN Appl Sci* 2:1838. <https://doi.org/10.1007/s42452-020-03637-7>
28. Braun K, Willenborg E, Schleifenbaum JH (2020) Laser polishing as a new post process for 3D-printed polymer parts. *Procedia CIRP* 94:134–138. <https://doi.org/10.1016/j.procir.2020.09.026>
29. Chryssolouris G (2013) *Laser machining: theory and practice*. Springer Science & Business Media, Springer Science & Business Media
30. Kechagias JD, Ninikas K, Salonitis K (2022) An experimental study of laser cutting of PLA-wood flour 3D printed plates using a modified Taguchi design. *Int J Exp Des Process Opt* 7:62–75. <https://doi.org/10.1504/IJEDPO.2022.131230>
31. Ninikas K, Kechagias J, Salonitis K (2021) The impact of process parameters on surface roughness and dimensional accuracy during CO₂ laser cutting of PMMA thin sheets. *J Manuf Mater Process* 5. <https://doi.org/10.3390/jmmp5030074>
32. Moradi M, Karami Moghadam M, Shamsborhan M, Bodaghi M, Falavandi H (2020) Post-processing of FDM 3D-printed polylactic acid parts by laser beam cutting. *Polymers (Basel)* 12:550. <https://doi.org/10.3390/polym12030550>
33. Kechagias J, Ninikas K, Petousis M, Vidakis N, Vaxevanidis N (2021) An investigation of surface quality characteristics of 3D printed PLA plates cut by CO₂ laser using experimental design. *Mater Manuf Process* 36:1544–1553. <https://doi.org/10.1080/10426914.2021.1906892>
34. Petousis M, Ninikas K, Vidakis N, Mountakis N, Kechagias JD (2023) Multifunctional PLA/CNTs nanocomposites hybrid 3D printing integrating material extrusion and CO₂ laser cutting. *J Manuf Process* 86:237–252. <https://doi.org/10.1016/j.jmapro.2022.12.060>
35. Stavropoulos P, Koutsomichalis A, Vaxevanidis N (2017) Laser-based manufacturing processes for aerospace applications. In: *Materials Science and Engineering*. IGI Global, pp 374–391. <https://doi.org/10.4018/978-1-5225-1798-6.ch014>
36. Steen WM (2003) Laser material processing - an overview. *J Opt A Pure Appl Opt* 5:S3–S7. <https://doi.org/10.1088/1464-4258/5/4/351>
37. Lambiase F, Genna S, Leone C (2020) Laser finishing of 3D printed parts produced by material extrusion. *Opt Lasers Eng* 124:105801. <https://doi.org/10.1016/j.optlaseng.2019.105801>
38. Choudhury IA, Shirley S (2010) Laser cutting of polymeric materials: an experimental investigation. *Opt Laser Technol* 42:503–508. <https://doi.org/10.1016/j.optlastec.2009.09.006>
39. Maurya HS, Kollo L, Tarraste M, Juhani K, Sergejev F, Prashanth KG (2022) Effect of the laser processing parameters on the selective laser melting of TiC–Fe-based cermets. *J Manuf Mater Proc* 6:35. <https://doi.org/10.3390/jmmp6020035>
40. Madić M, Mladenović S, Gostimirović M, Radovanović M, Janković P (2020) Laser cutting optimization model with constraints: maximization of material removal rate in CO₂ laser cutting of mild steel. *Proc Inst Mech Eng B J Eng Manuf* 234:1323–1332 <https://doi.org/10.1177/0954405420911529>
41. Martínez S, Lamikiz A, Ukar E, Calleja A, Arrizubieta JA, Lopez de Lacalle LN (2017) Analysis of the regimes in the scanner-based laser hardening process. *Opt Lasers Eng* 90. <https://doi.org/10.1016/j.optlaseng.2016.10.005>
42. Yilbas BS (1998) Study of Parameters for CO₂ laser cutting process. *Mater Manuf Proc* 13:517–536. <https://doi.org/10.1080/10426919808935273>
43. Manco E, Cozzolino E, Astarita A (2022) Laser polishing of additively manufactured metal parts: a review. *Surf Eng* 38:217–233. <https://doi.org/10.1080/02670844.2022.2072080>
44. Yue TM, Lau WS (1996) Pulsed Nd:YAG laser cutting of Al/Li/SiC metal matrix composites. *Mater Manuf Proc* 11:17–29. <https://doi.org/10.1080/10426919608947458>
45. Pandey AK, Dubey AK (2012) Taguchi based fuzzy logic optimization of multiple quality characteristics in laser cutting of duralumin sheet. *Opt Lasers Eng* 50:328–335. <https://doi.org/10.1016/j.optlaseng.2011.11.005>
46. Parandoush P, Tucker L, Zhou C, Lin D (2017) Laser assisted additive manufacturing of continuous fiber reinforced thermoplastic composites. *Mater Des* 131:186–195. <https://doi.org/10.1016/j.matdes.2017.06.013>
47. Kumar Pandey A, Kumar Dubey A (2012) Simultaneous optimization of multiple quality characteristics in laser cutting of titanium alloy sheet. *Opt Laser Technol* 44:1858–1865 <https://doi.org/10.1016/j.optlastec.2012.01.019>
48. Tewari R, Singh MK, Zafar S, Powar S (2021) Parametric optimization of laser drilling of microwave-processed kenaf/HDPE composite. *Polym Polym Compos* 29:176–187. <https://doi.org/10.1177/0967391120905705>
49. Davim JP, Barricas N, Conceição M, Oliveira C (2008) Some experimental studies on CO₂ laser cutting quality of polymeric materials. *J Mater Process Technol* 198:99–104. <https://doi.org/10.1016/j.jmatprotec.2007.06.056>
50. Kechagias JD, Fountas NA, Ninikas K, Petousis M, Vidakis N, Vaxevanidis N (2021) Surface characteristics investigation of 3D-printed PET-G plates during CO₂ laser cutting. *Mater Manuf Process*:1–11. <https://doi.org/10.1080/10426914.2021.1981933>
51. Kechagias J, Ninikas K, Petousis M, Vidakis N (2022) Laser cutting of 3D printed acrylonitrile butadiene styrene plates for dimensional and surface roughness optimization. *Int J Adv Manuf Technol* 119:2301–2315. <https://doi.org/10.1007/s00170-021-08350-2>
52. Fountas NA, Ninikas K, Chaidas D, Kechagias J, Vaxevanidis NM (2022) Neural networks for predicting kerf characteristics of CO₂ laser-machined FFF PLA/WF plates. *MATEC Web Conf* 368:01010. <https://doi.org/10.1051/mateconf/202236801010>
53. Kechagias JD, Vidakis N, Ninikas K, Petousis M, Vaxevanidis NM (2023) Hybrid 3D printing of multifunctional polylactic acid/carbon black nanocomposites made with material extrusion and post-processed with CO₂ laser cutting. *J Adv Manuf Technol* 124:1843–1861. <https://doi.org/10.1007/s00170-022-10604-6>
54. Alhawsawi AM, Moustafa EB, Fujii M, Banoqitah EM, Elsheikh A (2023) Kerf characteristics during CO₂ laser cutting of polymeric materials: experimental investigation and machine learning-based prediction. *Eng Sci Technol Int J* 46:101519. <https://doi.org/10.1016/j.jestch.2023.101519>
55. Anjum A, Shaikh A (2023) Experimental and analytical modeling for channel profile using CO₂ laser considering gaussian beam distribution. *Journal of Engineering Research* 11:100035. <https://doi.org/10.1016/j.jer.2023.100035>
56. Arthanari S, Park J-E, Heo JS, Cho DH, Yang M, Hwang JS, Lee H (2023) Laser surface polishing of 3D printed polylactic acid (PLA) with different levels of absorption. *J Manuf Process* 98:265–276. <https://doi.org/10.1016/j.jmapro.2023.05.034>
57. Ferreira SLC, Bruns RE, Ferreira HS, Matos GD, David JM, Brandão GC, da Silva EGP, Portugal LA, dos Reis PS, Souza AS, dos Santos WNL (2007) Box-Behnken design: an alternative for

- the optimization of analytical methods. *Anal Chim Acta* 597:179–186 <https://doi.org/10.1016/j.aca.2007.07.011>
58. Raj Mohan R, Venkatraman R, Raghuraman S (2021) Experimental analysis on density, micro-hardness, surface roughness and processing time of acrylonitrile butadiene styrene (ABS) through fused deposition modeling (FDM) using Box Behnken design (BBD). *Mater Today Commun* 27:102353. <https://doi.org/10.1016/j.mtcomm.2021.102353>
 59. Sharma P, Singh L, Dilbaghi N (2009) Optimization of process variables for decolorization of disperse yellow 211 by *Bacillus subtilis* using Box-Behnken design. *J Hazard Mater* 164:1024–1029. <https://doi.org/10.1016/j.jhazmat.2008.08.104>
 60. Tak B, Tak B, Kim Y, Park Y, Yoon Y, Min G (2015) Optimization of color and COD removal from livestock wastewater by electrocoagulation process: application of Box-Behnken design (BBD). *J Ind Eng Chem* 28:307–315 <https://doi.org/10.1016/j.jiec.2015.03.008>
 61. Goud V, Ramasamy A, Das A, Kalyanasundaram D (2019) Box-Behnken technique based multi-parametric optimization of electrostatic spray coating in the manufacturing of thermoplastic composites. *Mater Manuf Process* 34:1638–1645. <https://doi.org/10.1080/10426914.2019.1666991>
 62. Wu L, Yick K, Ng S, Yip J (2012) Application of the Box–Behnken design to the optimization of process parameters in foam cup molding. *Expert Syst Appl* 39:8059–8065 <https://doi.org/10.1016/j.eswa.2012.01.137>
 63. Jeganathan PM, Venkatachalam S, Karichappan T, Ramasamy S (2014) Model development and process optimization for solvent extraction of polyphenols from red grapes using Box-Behnken design. *Prep Biochem Biotechnol* 44:56–67. <https://doi.org/10.1080/10826068.2013.791629>
 64. Vinayagamoorthy R (2017) Parametric optimization studies on drilling of sandwich composites using the Box–Behnken design. *Mater Manuf Process* 32:645–653. <https://doi.org/10.1080/10426914.2016.1232811>
 65. Montgomery DC (2012) *Design and Analysis of Experiments*, 8th edn. Wiley, Hoboken, NJ, USA
 66. Lou H, Li W, Li C, Wang X (2013) Systematic investigation on parameters of solution blown micro/nanofibers using response surface methodology based on Box-Behnken design. *J Appl Polym Sci* 130:1383–1391. <https://doi.org/10.1002/app.39317>
 67. Zolgharnein J, Shahmoradi A, Ghasemi JB (2013) Comparative study of Box-Behnken, central composite, and Doehlert matrix for multivariate optimization of Pb (II) adsorption onto Robinia tree leaves. *J Chemom* 27:12–20. <https://doi.org/10.1002/cem.2487>
 68. Spahiu T, Kitsakis K, Kechagias J (2022) Box-Behnken design to optimise 3D printing parameters in applications for fashion products. *Int J Exp Des Proc Optim* 7:1. <https://doi.org/10.1504/IJEDPO.2022.10053016>
 69. Johnson RT, Montgomery DC (2009) Choice of second-order response surface designs for logistic and Poisson regression models. *Int J Exp Des Proc Optim* 1:2. <https://doi.org/10.1504/IJEDPO.2009.028954>

Publisher's Note Springer Nature remains neutral with regard to jurisdictional claims in published maps and institutional affiliations.